

PCCP

Accepted Manuscript



This is an *Accepted Manuscript*, which has been through the Royal Society of Chemistry peer review process and has been accepted for publication.

Accepted Manuscripts are published online shortly after acceptance, before technical editing, formatting and proof reading. Using this free service, authors can make their results available to the community, in citable form, before we publish the edited article. We will replace this *Accepted Manuscript* with the edited and formatted *Advance Article* as soon as it is available.

You can find more information about *Accepted Manuscripts* in the [Information for Authors](#).

Please note that technical editing may introduce minor changes to the text and/or graphics, which may alter content. The journal's standard [Terms & Conditions](#) and the [Ethical guidelines](#) still apply. In no event shall the Royal Society of Chemistry be held responsible for any errors or omissions in this *Accepted Manuscript* or any consequences arising from the use of any information it contains.

Cite this: DOI: 10.1039/c0xx00000x

www.rsc.org/xxxxxx

ARTICLE TYPE

Electronic Delocalization in Small Water Rings

Bo Wang,^{a,b} Minsi Xin,^{a,b} Xing Dai,^{a,b} Ruixia Song,^{a,b} Yan Meng,^{a,b} Jie Han,^{a,b} Wanrun Jiang,^{a,b} Zhigang Wang^{a,b} and Ruiqin Zhang^{a,c,d}

Received (in XXX, XXX) Xth XXXXXXXXX 20XX, Accepted Xth XXXXXXXXX 20XX

DOI: 10.1039/b000000x

Water clusters are known to form through hydrogen-bonding. However, this study shows that the formation of small water clusters such as (H₂O)_n of n=3 or 4 involves strong electron delocalization. Our first principles calculations reveal that the electron delocalization originates from both the H and O atomic orbitals and extends to the ring center, enriching the bonding characteristics of water clusters.

The Water clusters are the elementary structures and functional units of water. There has been consensus for some time that the origin of the formation of water clusters is dominated by hydrogen bonding (H-bonding), with water molecules gathering together by H-bonding networks.¹⁻³ It has been shown that stable water cluster structures are formed through complex H-bonding interaction.^{4, 5} Based on this understanding, numerous complex structures have been elucidated, including water rings, as have the functional characteristics of water clusters. The isolated single water ring (ISWR) is a typical closed system comprising n hydrogen bonds (H-bonds) formed by n water molecules.⁶ ISWR structures for n=3-5^{7, 8} have been experimentally demonstrated using far-infrared (IR) vibration-rotation tunneling (FIR-VRT) spectroscopy⁹ and IR laser spectroscopic technologies.¹⁰ For n=6, the ISWR structure reaches the maximum size and tends to change into a cage type with various geometric structures.^{11, 12} Quantum-mechanical level theoretical calculations have been used to study the conformations,^{5, 13, 14} energy,^{15, 16} IR or Raman spectroscopy,¹⁷ intramolecular vibrational redistribution and vibrational energy transfer,¹⁸ confined water structure and proton transport process,¹⁹ and so on of these structures. In particular, after differences between the results of adiabatic potential energy surface and experimental studies emerged,¹¹ there has been a closer collaboration between theoretical and experimental researchers.

So far, it is believed that for clusters with n<6, the cyclic structure has the lowest energy.^{8, 13} However, this may not represent a complete understanding, because although such structures are closed, the curvature of the circle for n=3 is larger than that for n=6 for the cases of n=3-6, leading to a considerably reduced O-H...O angle (∠OHO).^{6, 20} How is such a water ring stabilized? To explore the underlying mechanism, we carried out a detailed analysis of the electronic structure properties of cyclic structures n=3-6, with a particular focus on the mechanism of the bonding of the water rings at n=3 and 4. Our study was conducted using first-principles calculations of density functional theory

(DFT) methods with confirmations using post-Hartree-Fock and based on analyses of energy level diagram, electrostatic potential, electron density difference, reduced density gradient (RDG) and geometrical structure characteristics. We identify some characteristics of molecular orbitals (MOs), which are obviously related to cluster bonding and stability. We also show that the electronic delocalization effect is important in the interaction mechanism for n=3 and 4.

DFT methods have been shown to provide reliable results in studying the characteristics of water clusters and have been widely used.¹⁶ The inclusion of electron correlation effects means that DFT methods have an advantage in describing H-bonding interactions.^{21, 22} Although the post-Hartree-Fock approaches (such as second-order Møller-Plesset perturbation theory (MP2)²³ and coupled-cluster theory with single double (triple) excitations (CCSD(T)²⁴) can deal accurately with such interactions, they require considerably more computational resources, particularly the latter.²⁵

Among the various DFT methods, the hybrid Perdew-Burke-Ernzerhof (PBE0) functional²⁶⁻²⁸ is optimized to deal with the H-bonding interactions in water clusters using double-zeta basis sets.^{13, 14, 29} As the essence of H-bonding is intermolecular interaction, it is necessary to use polarization and diffuse functions in the basis set.^{13, 30, 31} We therefore used a 6-31+G(d, p) basis set for all atoms. All geometric structures were obtained using the PBE0 method. MP2 and M06-2X³² methods were also used for the purposes of comparison. All calculations were performed using the *Gaussian 09* package.³³

We obtained stable structures for n=3-6 using the structural optimization approach described in Part 1 of the Supplementary Information (SI) with the free H orientation also defined therein. Their infrared and Raman spectra calculated at the same level of theory are presented in SI (see Part 2 of the SI). We went on to analyze the electronic structures in order to explore their stability. Firstly, we calculated the energy level diagrams of water rings (see also the results of MP2 and M062X in Part 3 of the SI), and then examined its MO characteristics.

Figure 1 shows the energy level diagrams of water rings. The MOs with energies at the red line positions present delocalization characteristics crossing broad areas among the water molecules. Interestingly, the delocalized orbital is formed by the H and O atomic orbitals. The morphology of delocalized electron density is similar to that due to conventional hyperconjugation,^{34, 35} but is more likely induced by electron-deficiency that was found to

cause strong electron delocalization in silicon nanocrystals.³⁶ Here, as the number of n increases, the orbital energy differences of the characteristic MOs decrease. With an increase in the number of n , the molecular orbital tends to become more localized at the water ring. As a result, the corresponding molecular orbital of $n=5$ shows no electronic distribution in the central area. To examine the contribution of the O and H atomic orbitals to the delocalization of the MOs, we conducted a natural bond orbitals (NBO) analysis using the natural atomic orbitals (NAO) approach based on the calculated eigenstates (see the detailed analysis in Part 4 of the SI). We found that these orbitals are composed of the linear combination of the highest occupied MO HOMO-1($3a_1$) or HOMO-2($1b_2$) of the component water molecule (see part 5 of SI). The energy level of the characteristic orbital shifts up as the number of n increases.

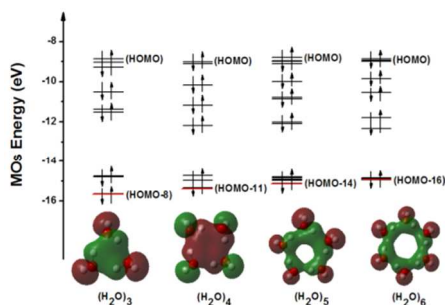


Figure 1. Energy level diagrams of the various water rings. The red lines correspond to the energy levels of the characteristic occupied MOs presented in the bottom diagram which were plotted using an isosurface value of 0.02 a.u.

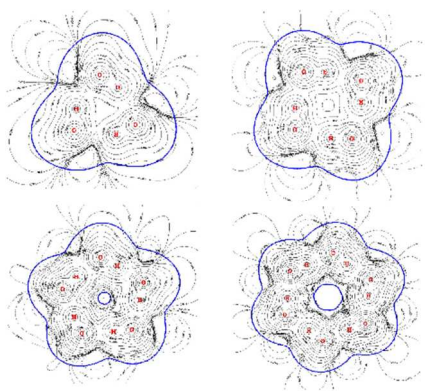


Figure 2. Electrostatic potentials of the water ring structures for $n=3-6$. The blue curve represents a van der Waals border and the red symbols the O and H atoms. The van der Waals boundary is found at an electron density equal to 0.001 a.u.

The electronic structural feature of the MOs of the water ring is similar to that of the electrostatic potential distribution. Figure 2 presents the electrostatic potential, which is defined as ϕ at a point r arising from M nuclei and the electron density ρ , and is calculated^{37, 38} by

$$\phi(r) = \sum_{a=1}^M \frac{Z_a}{|R_a - r|} - \int \frac{\rho(r')}{|r' - r|} dr'$$

Here R_a and Z_a are the position and the charge, respectively, of nucleus a . The electron is distributed throughout the central

region at $n=3$ and 4, which is consistent with the energy level diagram result. This also shows that the presence of a stable water ring structure depends on intermolecular H-bonding and electron delocalization in the central region. Starting from $n=5$, the van der Waals boundary appears at the ring center (where the electron density is less than 0.001). Hence, the electron bonding is not strong enough for the area outside the van der Waals boundary to be considered as a weak interaction region between electrons. As the n increases, the central area (that is, the van der Waals boundary expansion) enlarges, which is consistent with the change in the energy level diagrams.

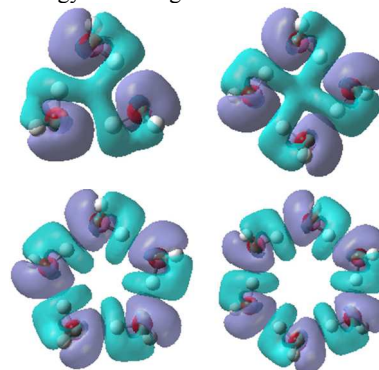


Figure 3. Isosurface of the electron density difference for water ring structures of $n=3-6$. The blue region represents the electron donor and the purple region the electron acceptor. The isosurface value is ± 0.0004 .

The characteristics of the orbital delocalization mainly reflect the electronic distribution. To confirm the differences found in the orbital delocalization, we also calculated the electron density difference (see Figure 3), which are defined as $\rho = \rho_{\text{Total}} - \sum \rho_{\text{Molecule}}$ where ρ_{Total} is the electron density of the water ring and ρ_{Molecule} is the electron density of each water molecule. It is clear that the O atoms gain electrons and the H atoms lose them. There is also a similarity in the characteristics of the orbital delocalization. From these analyses of the electrostatic potential and electron density difference, we can see that compared to the case of $n=5$, the electron delocalization for $n=3$ and 4 extends over the whole region. The delocalized electron density of the central region decreases as the number of n increases. The electrons tend to localize on the water molecules. Such delocalization characteristics involving hydroxides have been observed experimentally in an intermolecular bonding system (copper crystal surface binding on the dehydrogenated hydroxyquinoline molecule).³⁹ This indicates that the interaction mechanism of the water ring ($n=3$ and 4) is different from that of other cluster structures ($n>4$).

In order to further understand the interaction mechanism of ISWR with $n=3$ and 4, we next investigated the RDG of these systems. The RDG is defined as: $s = 1 / (2(3\pi^2)^{1/3}) |\nabla \rho| / \rho^{4/3}$, where ρ is the electron density. Figure 4 displays the gradient ($s=0.6$ a.u.) isosurfaces, where the colors of the gradient isosurfaces are a good indicator of the interaction strength. The green areas in the centers of the water rings with $n=3$ and 4 as well as those between the intermolecular H-bonding regions indicate where strong van der Waals interactions present. It is seen that the van der Waals interactions reduce with the increase of n . The analysis also shows an obvious difference between the

RDG of the two smallest water rings and those of the other water rings. The similar conclusions have been confirmed by the nuclear independent chemical shift (NICS) study (see Part 6 of SI).

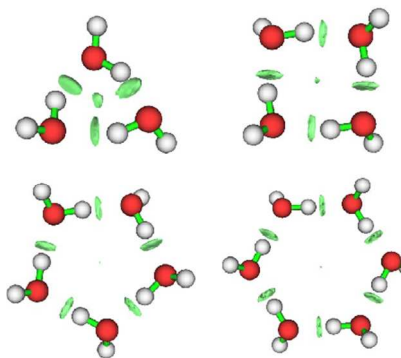


Figure 4. Gradient isosurface ($s=0.6$ a.u.). The green color indicates the strength of van der Waals interactions.

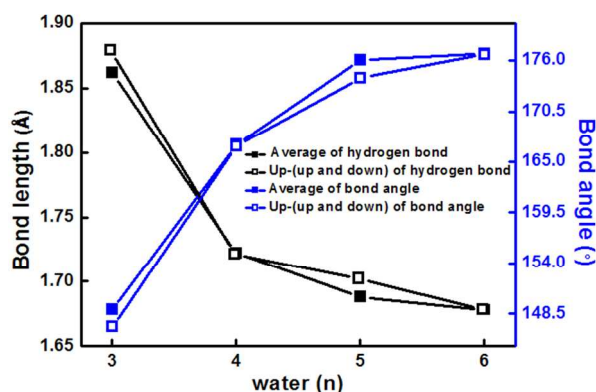


Figure 5. Geometric structure parameters for water rings of $n=3-6$. The black (blue) solid squares represent the average H-bond length (bond angle), the black (blue) open squares represent the up-(up and down) H-bond length (bond angle). There is no up-up H atom when n is an even number, so the empty and solid squares are at the same point.

Since the geometric structure of H-bonds can be a good indicator of the stability of the system,^{6,20} we selected the first of the two H atoms with the same orientation as the starting point to count all the H-bond lengths of R_{hb} (the distance between the donor H and acceptor O atoms) and bond angle Φ (H-bond angle O-H...O) in the counterclockwise direction. We note that there are two H atoms found in the water ring with an odd number of molecules (see Part 1 of the SI). In contrast, there is no H atom with the same orientation in the water ring structure with an even number of molecules, and the H-bonds in these rings are all the same. As shown in Figure 5, an increase in the number of n leads to a gradual decrease in the average and up-(up and down) H-bond lengths for $n=3-6$, which is consistent with the literature.⁴⁰ NBO analysis shows that the stabilization energy $E(2)$ increases gradually with the increase of the number of water molecules. This interaction causes reduction in H-bond lengths (see the detailed analysis in Part 7 of the SI). With a gradual increase in the average and up-(up and down) bond angles, as shown previously,^{6,20} A more detailed analysis can be found in Part 8 of the SI. The H-bond length and angle also shows an interesting

rapid change, consistent with the characteristic changes in electronic structure in the $n=3$ and 4 systems. The variation in the NBO and Mulliken charges follows a similar trend. The results are shown in Part 9 of the SI.

Conclusions

In summary, using first-principles DFT method, we have studied the stable mechanism of small water ring. Analysis showed obvious delocalized electronic characteristics in the two smallest water rings ($n=3$ and 4). In particular, there are obvious differences in the energy level diagram, electrostatic potential, density, RGD, and H-bonding geometric structures compared with larger rings. These results form an important point of reference for investigation of the H-bonding nature and structural properties of water clusters. It is worth noting that recent experiments demonstrate similar features in terms of the electronic cloud overlapping in H-bond regions.⁴¹ There have been also indications of the influence of H-bonding on the local electronic structure of liquid water.⁴² The covalent-like properties of an 8-hydroxyquinoline molecule assembled on a Cu(111) substrate using noncontact atomic force microscopy (NC-AFM) have also been observed.³⁹ Our work significantly reflects the delocalized electronic distribution characteristics related to H-bonding.

Acknowledgements

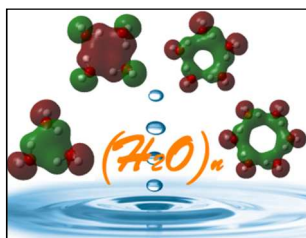
The work was supported by the National Basic Research Program of China (973 Program), the National Science Foundation of China (under grant numbers 11374004 and 11004076) and Science and Technology Development Program of Jilin Province of China (20150519021JH). Z. W. also acknowledges the assistance of the Fok Ying Tung Education Foundation (142001) and the High Performance Computing Center of Jilin University.

Notes and references

- ^a Institute of Atomic and Molecular Physics, Jilin University, Changchun, 130012, China
 - ^b Jilin Provincial Key Laboratory of Applied Atomic and Molecular Spectroscopy (Jilin University), Changchun, 130012, China
 - ^c Department of Physics and Materials Science and Centre for Functional Photonics (CFP), City University of Hong Kong, Hong Kong SAR, China
 - ^d Beijing Computational Science Research Center, Beijing 100084, China
- *To whom correspondence should be addressed. E-mail: wangzg@jlu.edu.cn; aprqz@cityu.edu.hk
- †Electronic Supplementary Information (ESI) available: See DOI: 10.1039/b000000x/
- B. Santra, A. Michaelides, M. Fuchs, A. Tkatchenko, C. Filippi and M. Scheffler, *J. Chem. Phys.*, 2008, **129**, 194111.
 - E. E. Dahlke and D. G. Truhlar, *J. Phys. Chem. B*, 2005, **109**, 15677.
 - T. Todorova, A. P. Seitsonen, J. Hutter, I. F. W. Kuo and C. J. Mundy, *J. Phys. Chem. B*, 2006, **110**, 3685.
 - J. Sadlej, V. Buch, J. K. Kazimirski and U. Buck, *J. Phys. Chem. A*, 1999, **103**, 4933.
 - S. Maheshwary, N. Patel, N. Sathyamurthy, A. D. Kulkarni and S. R. Gadre, *J. Phys. Chem. A*, 2001, **105**, 10525.
 - S. S. Xantheas, *J. Chem. Phys.*, 1995, **102**, 4505.
 - N. Pugliano and R. J. Saykally, *Science*, 1992, **257**, 1937.

- 8 J. K. Gregory, D. C. Clary, K. Liu, M. G. Brown and R. J. Saykally, *Science*, 1997, **275**, 814.
- 9 N. Pugliano and R. J. Saykally, *Science*, 1937(1992), **257**,
- 10 F. Huisken, M. Kaloudis and A. Kulcke, *J. Chem. Phys.*, 1996, **104**,
- 5 17.
- 11 R. J. Saykally and D. J. Wales, *Science*, 2012, **336**, 814.
- 12 K. Liu, M. G. Brown, C. Carter, R. J. Saykally, J. K. Gregory and D. C. Clary, *nature*, 1996, **381**, 501.
- 13 R. M. Shields, B. Temelso, K. A. Archer, T. E. Morrell and G. C. Shields, *J. Phys. Chem. A*, 2010, **114**, 11725.
- 10 14 M. Losada and S. Leutwyler, *J. Chem. Phys.*, 2002, **117**, 2003.
- 15 B. Temelso, K. A. Archer and G. C. Shields, *J. Phys. Chem. A*, 2011, **115**, 12034.
- 16 J. T. Su, X. Xu and W. A. Goddard, *J. Phys. Chem. A*, 2004, **108**,
- 15 10518.
- 17 R. Knochenmuss and S. Leutwyler, *J. Chem. Phys.*, 1992, **96**, 5233.
- 18 Y. L. Niu, R. Pang, C. Y. Zhu, M. Hayashi, Y. Fujimura, S. H. Lin and Y. R. Shen, *Chem. Phys. Lett.*, 2013, **586**, 153.
- 19 P. Hirunsit and P. B. Balbuena, *J. Phys. Chem. A*, 2007, **111**, 10722.
- 20 S. S. Xantheas and T. H. Dunning Jr, *J. Chem. Phys.*, 1993, **99**, 8774.
- 21 B. Kolb and T. Thonhauser, *Phys. Rev. B*, 2011, **84**, 045116.
- 22 F. Li, L. Wang, J. Zhao, J. R. H. Xie, K. E. Riley and Z. Chen, *Theor. Chem. Acc.*, 2011, **130**, 341.
- 23 C. Møller and M. S. Plesset, *Phys. Rev.*, 1934, **46**, 618.
- 24 J. A. Pople, M. Head - Gordon and K. Raghavachari, *J. Chem. Phys.*, 1987, **87**, 5968.
- 25 S. Tsuzuki and H. P. Lüthi, *J. Chem. Phys.*, 2001, **114**, 3949.
- 26 C. Adamo and V. Barone, *J. Chem. Phys.*, 1999, **110**, 6158.
- 27 J. P. Perdew, K. Burke and M. Ernzerhof, *Phys. Rev. Lett.*, 1996, **77**, 3865.
- 28 M. Ernzerhof and G. E. Scuseria, *J. Chem. Phys.*, 1999, **110**, 5029.
- 29 J. R. Hammond, N. Govind, K. Kowalski, J. Autschbach and S. S. Xantheas, *J. Chem. Phys.*, 2009, **131**, 214103.
- 30 E. E. Dahlke, R. M. Olson, H. R. Leverentz and D. G. Truhlar, *J. Phys. Chem. A*, 2008, **112**, 3976.
- 31 Y. Ghadar and A. E. Clark, *J. Chem. Phys.*, 2012, **136**, 054305.
- 32 Y. Zhao and D. G. Truhlar, *Theor. Chem. Acc.*, 2008, **120**, 215.
- 33 M. J. Frisch, G. W. Trucks, H. B. Schlegel, G. E. Scuseria, M. A. Robb, J. R. Cheeseman, G. Scalmani, V. Barone, B. Mennucci, G. A. Petersson, H. Nakatsuji, M. Caricato, X. Li, H. P. Hratchian, A. F. Izmaylov, J. Bloino, G. Zheng, J. L. Sonnenberg, M. Hada, M. Ehara, K. Toyota, R. Fukuda, J. Hasegawa, M. Ishida, T. Nakajima, Y. Honda, O. Kitao, H. Nakai, T. Vreven, J. A. Montgomery, J. E. Peralta, F. Ogliaro, M. Bearpark, J. J. Heyd, E. Brothers, K. N. Kudin, V. N. Staroverov, T. Keith, R. Kobayashi, J. Normand, K. Raghavachari, A. Rendell, J. C. Burant, S. S. Iyengar, J. Tomasi, M. Cossi, N. Rega, J. M. Millam, M. Klene, J. E. Knox, J. B. Cross, V. Bakken, C. Adamo, J. Jaramillo, R. Gomperts, R. E. Stratmann, O. Yazyev, A. J. Austin, R. Cammi, C. Pomelli, J. W. Ochterski, R. L. Martin, K. Morokuma, V. G. Zakrzewski, G. A. Voth, P. Salvador, J. J. Dannenberg, S. Dapprich, A. D. Daniels, O. Farkas, J. B. Foresman, J. V. Ortiz, J. Cioslowski and D. J. Fox, *Gaussian 09 (Revision D.01)*, Gaussian, Inc., Wallingford, CT, 2013
- 34 Y. Meng, C. Tian, F. Wang, Z. Wang, M. Jin, L. Chen, W. Feng and D. Ding, *J. Theor. Comput. Chem.*, 2012, **11**, 1217.
- 35 L. Goodman and R. R. Sauer, *J. Chem. Theory Comput.*, 2005, **1**, 1185.
- 36 H. Vach, *Nano. Lett.*, 2011, **11**, 5477.
- 37 S. Jakobsen, K. Kristensen and F. Jensen, *J. Chem. Theory Comput.*, 2013, **9**, 3978.
- 38 T. Lu and F. Chen, *J. Comp. Chem.*, 2012, **33**, 580.
- 39 J. Zhang, P. Chen, B. Yuan, W. Ji, Z. Cheng and X. Qiu, *Science*, 2013, **342**, 611.
- 40 C. Q. Sun, X. Zhang, J. Zhou, Y. L. Huang, Y. Zhou and W. Zheng, *J. Phys. Chem. Lett.*, 2013, 2565.
- 41 E. Espinosa, C. Lecomte and E. Molins, *Chem. Phys. Lett.*, 1999, **300**, 745.
- 42 J. H. Guo, Y. Luo, A. Augustsson, J. E. Rubensson, C. Sâthe, H. gren and J. Nordgren, *Phys. Rev. Lett.*, 2002, **89**, 137402.

Table of Contents



Delocalized molecular orbitals of water rings (n=3-6).

Cite this: DOI: 10.1039/c0xx00000x

www.rsc.org/xxxxxx

ARTICLE TYPE

Supplementary Information

Supporting Information for the paper entitled “Electronic Delocalization in Small Water Rings” by Bo Wang, Minsi Xin, Xing Dai, Ruixia Song, Yan Meng, Jie Han, Wanrun Jiang, Zhigang Wang* and Ruiqin Zhang*.

1. The isolated single water ring (ISWR) initial structures
2. Water cluster vibrational characteristics in infra-red (IR) and Raman spectra
3. Energy level diagrams from MP2 and M062X calculations
4. Results of the population analysis of the molecular orbitals
5. Molecular orbitals contribution of the isolated water molecule
6. Nuclear independent chemical shift (NICS) zz curves of water rings for n=3-6
7. Second order perturbation theory analysis of Fock matrix with NBO basis
8. Analysis of hydrogen (H)-bond lengths and angles
9. Analysis of the Natural Bond Orbitals (NBO) and Mulliken charges of oxygen (O) atoms in water clusters
10. References for supplementary information

1. The ISWR initial structures

To prepare the calculations and analyses of the ISWR, we first built initial structures containing virtual atoms (see Figure S2) in order to allow the O atom at the same plane to relax. The exo-ring H of the structures containing an even number of water molecules lie in the up-down position (an unusual orientation for H) with respect to the stable main structure, while the corresponding H atoms in structures comprising an odd number of water molecules exist at the up-up position in a stable structure.

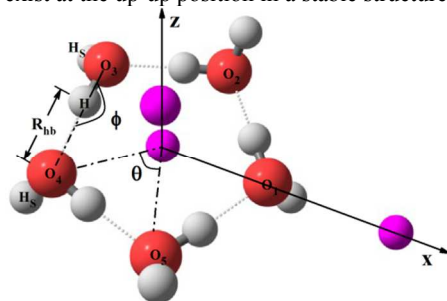


Figure S1 Schematic diagram of a typical ISWR structure (O in red, H in white, H-bonds along the grey dotted lines and three virtual atoms in pink).

To unify the numbering, we label the H-bond in the water molecule containing O₃ pointing to the O₄ as the first H-bond and the numbers of the other H-bonds in the ring increase in the counterclockwise direction. In this work, all statistics are performed according to this definition. R_{hb} represents the H-bond distance between the donor H and acceptor O atoms, ϕ the bond angle ($\angle\text{OHO}$), θ the central angle formed by the two O atoms and one virtual atom, H_s the H atoms with the same orientation, H the H atom forming the H-bond, and O₁-O₅ the water molecules, numbered beginning with the one at the X axis. The reference axes are established based on the positional relationships of the three virtual atoms (rendered in pink).

2. Water cluster vibrational characteristics in the IR and Raman spectra

IR and Raman spectroscopies are widely used to describe the structural properties of water clusters. We calculated the vibration spectra of stable water ring structures with n=3-6 and obtained their Raman and IR spectra. These were consistent with previous reports.^{8,S1,S2} The corresponding peak frequencies of the Raman spectra are 3569.8 cm⁻¹, 3498.7 cm⁻¹, 3255.00 cm⁻¹, and 3234.9 cm⁻¹ for n=3-6, respectively, as shown in Figure S2a. These peaks have the same vibration mode; that is, the overall H-bond stretching mode. We found that the highest peak presented a red shift with the increase in the number of water molecules (n) when n≤6, indicating a trend for the bond strength to decline.

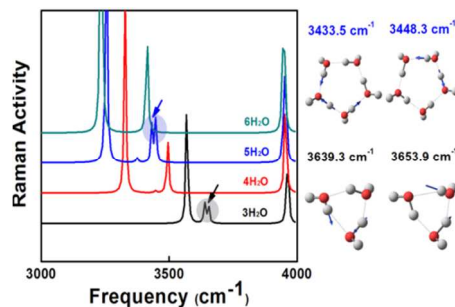


Figure S2a The solid lines, from bottom to top, denote the Raman spectra for the water rings of $(\text{H}_2\text{O})_3$, $(\text{H}_2\text{O})_4$, $(\text{H}_2\text{O})_5$, and $(\text{H}_2\text{O})_6$. The shadow areas indicated by the blue and black arrows represent the characteristic peaks of two kinds of ring structures. The right panel illustrates the four spectral vibrational modes of the water ring for $(\text{H}_2\text{O})_3$ and $(\text{H}_2\text{O})_5$, and the corresponding modes can be found in the left panel.

In Figure S2a, the shaded areas of the peaks to which the black and blue arrows point correspond to the characteristic water ring vibration modes for $n=3$ and 5 (see Figure S2a for the vibration mode diagram in the right panel). The peaks of the black curve of 3639.3 cm^{-1} and the blue curve of 3433.5 cm^{-1} , respectively, correspond to the OH bonds stretching away from the water molecules with the same orientations. The peaks of the black curve at 3653.9 cm^{-1} and the blue curve at 3448.3 cm^{-1} , respectively, are the OH bond stretching modes from the water molecules with the same orientation. Compared with the Raman spectroscopy, the IR spectroscopy also shows some qualitative trends.

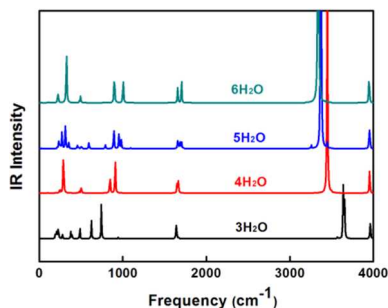


Figure S2b The solid curves, from bottom to top, denote the IR spectra for the water rings of $(\text{H}_2\text{O})_3$, $(\text{H}_2\text{O})_4$, $(\text{H}_2\text{O})_5$, and $(\text{H}_2\text{O})_6$.

In Figure S2b, the peaks of the IR spectra can be classified into three regions; (1) the vibration modes below 1100 cm^{-1} corresponding to the relative movements between the water molecules and the OH bond of water in an intramolecular asymmetric twist; (2) the vibration mode in the range $1000\text{--}2000 \text{ cm}^{-1}$ denotes the symmetrical swing of the H and O atoms; and (3) the main vibrational mode in the frequency above 3000 cm^{-1} represents the stretching modes between the intermolecular and intramolecular form of the OH bond. The highest peaks of the water ring structures are found at the frequencies 3639.3 cm^{-1} , 3447.3 cm^{-1} , 3366.0 cm^{-1} , and 3337.9 cm^{-1} , respectively. They have the same vibrational modes corresponding to the vibration of the OH bonds. We can see that the highest peaks show red shifts as the number of water molecules increases toward 6.

3. Energy level diagrams from MP2 and M062X calculations

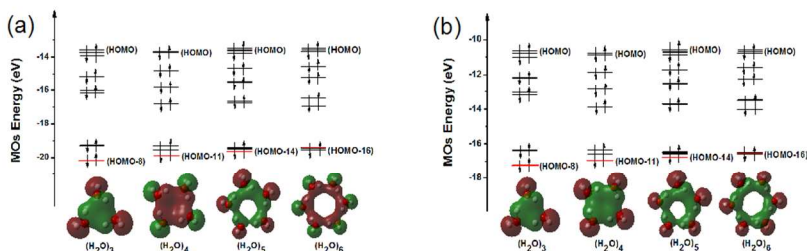


Figure S3 The energy level diagrams of water clusters from MP2(a) and M062X(b) calculations.

Figures S3a and S3b represent the MP2 and M062X calculation results including the energy levels of water rings and selected characteristic occupied MOs. The energy levels of the latter are marked with red lines in the diagram. The isosurface value of the orbital diagram is 0.02 a.u. As shown in Figure S3, the features of the energy level diagram and the trend of the orbitals in the two sets of results are consistent and also consistent with those obtained from PBE0 calculations.

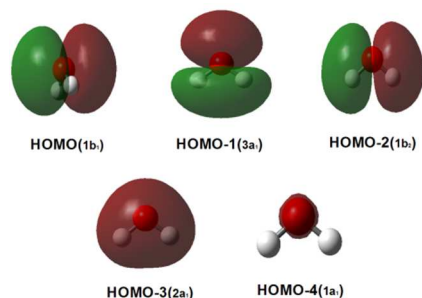
4. Results of the Population Analysis of the Molecular Orbitals

Table S1 The atomic orbital contribution percentages in HOMO-(8,11,14,16) correspond to the special molecular orbitals indicated in Figure 1 of the $(\text{H}_2\text{O})_3$, $(\text{H}_2\text{O})_4$, $(\text{H}_2\text{O})_5$, and $(\text{H}_2\text{O})_6$. p represents the valence orbital contribution of an O atom, s_{H} the s-orbital contribution of an H atom forming the H-bond, and s the s-orbital contribution of the free H atom.

$(\text{H}_2\text{O})_3$ (HOMO-8)			$(\text{H}_2\text{O})_4$ (HOMO-11)			$(\text{H}_2\text{O})_5$ (HOMO-14)			$(\text{H}_2\text{O})_6$ (HOMO-16)		
O (%)	H (%)		O (%)	H (%)		O (%)	H (%)		O (%)	H (%)	
2p	$1s_{\text{H}}$	1s	2p	$1s_{\text{H}}$	1s	2p	$1s_{\text{H}}$	1s	2p	$1s_{\text{H}}$	1s
76.01	10.17	13.37	76.29	9.56	13.72	76.37	9.30	13.88	76.64	10.01	12.89

Their contribution percentages are listed in Table S1. The linear combination of the molecular orbitals of different fragments (that is, 5 different water molecules) gives the molecular orbital structure shown in Figure S4, where the p-orbital component also varies due to the structural differences. From the orbital analysis, the total contribution made by the 2p and 1s orbital electrons is basically the same as that of the isolated water molecule in Figure S4.

5. Molecular orbitals contribution of the isolated water molecule

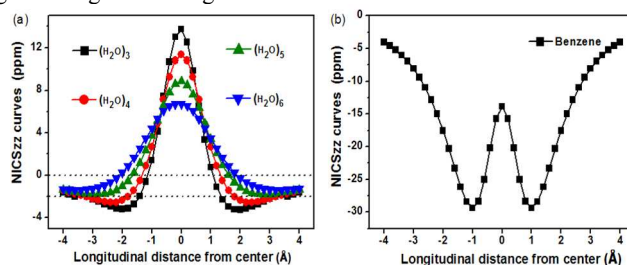


10 Figure S4 The molecular orbitals of the isolated water molecule.

The n th orbital below the highest occupied molecular orbital (HOMO) is denoted by HOMO- n . The corresponding irreducible representation of the molecular orbitals is also shown in Figure S4. The results of the calculation are consistent with recent experimental 15 data.^{S3} It can clearly be seen that the molecular orbital in Figure 1 is HOMO-2 which is a linear combination of H and O atomic orbitals. The 2p orbital contribution of the O atom accounts for about 74.32% of the OH bond, and the 1s orbital contributions of the two H atoms are about 12.62% and 12.62%, respectively.

6. Nuclear independent chemical shift (NICS) zz curves of water rings for $n=3-6$

20 NICS and NICSzz values are widely used to probe the aromaticity in electron delocalized systems, with the latter being more reliable.^[S4,S5,S6] Here we constructed NICSzz curves of water rings for $n=3-6$ and benzene (C_6H_6), which are shown in Figures S5a and S5b, respectively. The NICSzz curve of benzene is given as a common reference, and it is consistent with previous studies.^[S7,S8] Different from benzene, water rings show antiaromaticities around centers of rings and aromaticities at other regions. Both antiaromaticity and aromaticity decrease with the increase of number (n) of water molecules. The trend also involves some difference between the cases of 25 $n=3$ and 4 and $n=5$ and 6 (see Fig. S5a). Each of the cases of $n=3$ and 4 presents a valley at about 2 Å from the center of the water ring, showing the region with maximum aromaticity. But, the valley is hardly observed in the curves of $n=5$ and 6. This further illustrates the difference between small water rings and large water rings.



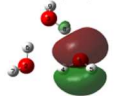
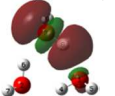
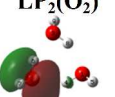
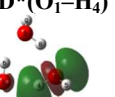
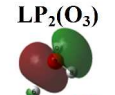
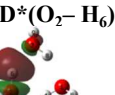
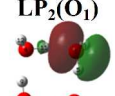
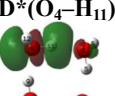
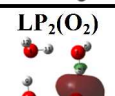
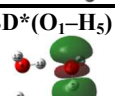
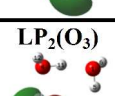
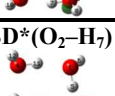
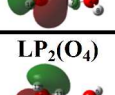
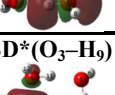
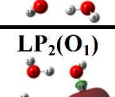
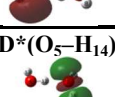
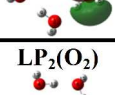
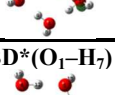
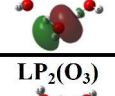
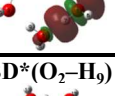
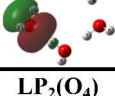
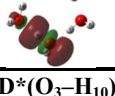
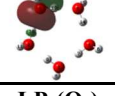
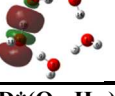
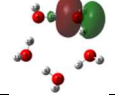
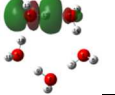
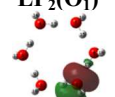
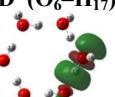
30 Figure S5. Nuclear independent chemical shifts (NICS) as function of the longitudinal distance from the center of the water rings for $n=3-6$ (Figure S1a) and benzene (C_6H_6 ; Figure S1b), respectively.

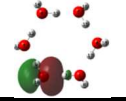
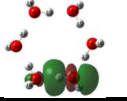
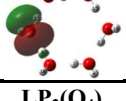
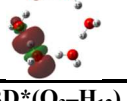
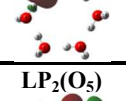
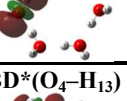
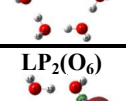
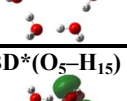
7. Second order perturbation theory analysis of Fock matrix with NBO basis

We performed a complete NBO analysis. The large values of stabilization energy $E(2)$ are presented in Table S2. NBO analysis shows that the stabilization energy $E(2)$ increases gradually with the increase of the number of water molecules. This interaction weakens the O- 35 H bond and elongates the O-H (namely, contracted O...H). This result is in agreement with the previous studies,^[S9,S10] and the trend is consistent with the previous one that the H-bond length decreases gradually with the increase of the number of water molecules.^[6,20]

Table S2. Second order perturbation theory analysis of Fock matrix with NBO basis.

Donor (i)	Nature orbital occupancy	Acceptor (j)	$E(2)^a$ (kJ/mol)	$E(j) - E(i)^b$ (a.u.)	$F(i,j)^c$ (a.u.)
-----------	--------------------------	--------------	----------------------	---------------------------	----------------------

$(\text{H}_2\text{O})_3$	LP ₂ (O ₁)	1.96832	BD*(O ₃ -H ₈)	14.75	1.01	0.109
						
	LP ₂ (O ₂)	1.97127	BD*(O ₁ -H ₄)	13.06	1.01	0.103
						
	LP ₂ (O ₃)	1.96725	BD*(O ₂ -H ₆)	14.93	0.99	0.109
						
$(\text{H}_2\text{O})_4$	LP ₂ (O ₁)	1.94891	BD*(O ₄ -H ₁₁)	25.53	1.01	0.144
						
	LP ₂ (O ₂)	1.94882	BD*(O ₁ -H ₅)	25.63	1.02	0.144
						
	LP ₂ (O ₃)	1.94877	BD*(O ₂ -H ₇)	25.67	1.02	0.144
						
	LP ₂ (O ₄)	1.94886	BD*(O ₃ -H ₉)	25.61	1.02	0.144
						
$(\text{H}_2\text{O})_5$	LP ₂ (O ₁)	1.94289	BD*(O ₅ -H ₁₄)	29.48	1.04	0.156
						
	LP ₂ (O ₂)	1.94255	BD*(O ₁ -H ₇)	29.54	1.03	0.156
						
	LP ₂ (O ₃)	1.94395	BD*(O ₂ -H ₉)	29.11	1.05	0.156
						
	LP ₂ (O ₄)	1.94691	BD*(O ₃ -H ₁₀)	27.34	1.06	0.152
						
	LP ₂ (O ₅)	1.94273	BD*(O ₄ -H ₁₂)	29.41	1.03	0.156
						
$(\text{H}_2\text{O})_6$	LP ₂ (O ₁)	1.93329	BD*(O ₆ -H ₁₇)	34.31	1.01	0.166
						
	LP ₂ (O ₂)	1.93367	BD*(O ₁ -H ₇)	34.12	1.01	0.166
						

	LP ₂ (O ₃)	1.93339		BD*(O ₂ -H ₉)	34.20	1.01	0.166
	LP ₂ (O ₄)	1.93355		BD*(O ₃ -H ₁₂)	34.16	1.01	0.166
	LP ₂ (O ₅)	1.99727		BD*(O ₄ -H ₁₃)	34.24	1.01	0.166
	LP ₂ (O ₆)	1.93340		BD*(O ₅ -H ₁₅)	34.23	1.01	0.166

^a E(2) stands for the stabilization energy. ^b energy difference between donor and acceptor (i_{th} and j_{th} NBO orbitals). ^c F(i,j) is the Fock matrix element between i_{th} and j_{th} NBO orbitals.

8. Analysis of H-bond lengths and angles

Table S3 H-bond length R_{oh} (Å)

(H ₂ O) ₃	1.879	1.853	1.853			
(H ₂ O) ₄	1.721	1.721	1.721	1.723		
(H ₂ O) ₅	1.702	1.685	1.684	1.684	1.686	
(H ₂ O) ₆	1.678	1.678	1.678	1.677	1.677	1.677

Table S4 Bond angle (\angle O-H...O) Φ (°)

(H ₂ O) ₃	147.2	149.9	149.8			
(H ₂ O) ₄	166.8	166.9	166.8	167.1		
(H ₂ O) ₅	174.2	177.0	176.2	176.4	176.5	
(H ₂ O) ₆	176.8	176.8	176.8	176.8	176.8	176.8

In Table S3, the data in the columns and diagonals (enclosed with dashed lines) increase as the number of water molecules decreases. The decrease in H-bond lengths for $n=3-6$ is consistent with previous results.^{6,20} As we can see from the column and diagonal terms (enclosed with dashed lines) in Table S4, the bond angle Φ (\angle OH...O) increases gradually with the increase of the number of water molecules.^{6,20}

9. Analysis of the Mulliken and NBO charges of O atoms in water clusters

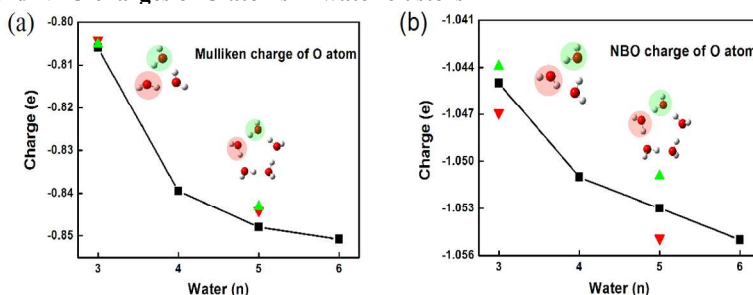


Figure S6 (a, b) represent the Mulliken and NBO charges of the O atom.

The black boxes represent the average Mulliken (or NBO) charges of the O atoms at $n = (4,6)$ or the average Mulliken (or NBO) charges for the removal of the O atoms of the same orientation at $n=3$ and 5. The red and green areas represent the Mulliken (or NBO) charges of the O atom in the same orientation. Figure S6 (a, b) shows the Mulliken and NBO charges of the O atom, which demonstrate a similar trend for $n=3-6$. However, the Mulliken or NBO charges of the O atom show an obvious change at $n=3$ and 4.

5

10. References for Supplementary Information

- S1. J. R. Reimers and R. O. Watts, *Chem. Phys.* 1984, **85**, 83.
S2. H. Cybulski, and J. Sadlej, On the calculations of the vibrational Raman spectra of small water clusters. *Chem. Phys.* 2007, **324**, 163.
S3. J. Guo, X. Meng, J. Chen, J. Peng, J. Sheng, X. Z. Li and Y. Jiang, *Nat. Mater.* 2014, **13**, 184.
10 S4. J. Yu, Q. Sun, Y. Kawazoe, P. Jena, *Nanoscale*, 2014, **6**, 14962.
S5. R. Gershoni - Poranne, A. Stanger, *Chem.-Eur. J.*, 2014, **20**, 5673.
S6. A. C. Tsipis, *Phys. Chem. Chem. Phys.*, 2009, **11**, 8244.
S7. A. Stanger, *J. Org. Chem.* 2006, **71**, 883.
S8. Z. Chen, C. S. Wannere, C. Corminboeuf, R. Puchta, P. V. R. Schleyer, *Chem. Rev.*, 2005, **105**, 3842.
15 S9. J. Chocholoušová, V. Špirko, P. Hobza, *Phys. Chem. Chem. Phys.*, 2004, **6**, 37.
S10. S. V. C. Vummaleti, D. Branduardi, M. Masetti, M. De Vivo, R. Motterlini, A. Cavalli, *Chem.-Eur. J.*, 2012, **18**, 9267.